Performance Bounds for Velocity Estimation With Extremely Large Aperture Arrays

Caterina Giovannetti, *Graduate Student Member, IEEE*, Nicolò Decarli, *Member, IEEE*, and Davide Dardari, *Senior Member, IEEE*

***Abstract*—Joint communication and sensing (JCS) is envisioned as an enabler of future 6G networks. One of the key features of these networks will be the use of extremely large aperture arrays (ELAAs) and high operating frequencies, which will result in significant near-field propagation effects. This unique property can be harnessed to improve sensing capabilities. In this letter, we focus on velocity sensing, as using ELAAs allows the estimation of not just the radial velocity component but also the transverse component. We derive analytical performance bounds for both velocity components, demonstrating how they are affected by the different system parameters and geometries. These results offer insights providing a foundational understanding of how near-field effects play in velocity sensing differently from the far field and from position estimate.**

***Index Terms*—Velocity estimation, Doppler, near field radar, extremely large aperture arrays (ELAAs), Cramér-Rao lower bound (CRLB), joint communication and sensing (JCS).**

I. Introduction

JOINT communication and sensing (JCS) is a technology that combines wireless data communication with radar sensing into a single system. Instead of using separate hardware and spectrum for each function, JCS enables devices to communicate and sense at the same time, often using the same signals and frequency bands. This integration improves spectrum efficiency, reduces hardware costs, opens new applications, and it has been identified as a pillar for the forthcoming 6G [1]. Among the quantities that can be sensed concerning a passive target, Doppler-based velocity estimation relies on the principle that the frequency of a propagating wave changes when the target and the observer are in motion relative to each other [2]. By analyzing the frequency variations, radar systems can determine whether a target is approaching or receding and at what speed. However, only the radial velocity, i.e., the projection of the target velocity along the target-receiver direction, can produce frequency variations under traditional far-field operating conditions [2].

Recently, communication systems are shifting towards the adoption of extremely large aperture arrays (ELAAs) and high carrier frequencies, making traditional far-field assumptions for propagation no longer fulfilled [3]. In the last years, this operating condition has been deeply investigated for what concerns communication and localization [4], [5]. In the field of radar sensing, studies are still at the early stage and usually focus on the enhanced resolution offered in terms of distance/angle estimation [6], [7], [8]. When dispersed antennas are employed, the ability to observe targets from different directions permits the estimation of the different velocity components using multi-static radars [9]. However, thanks to the adoption of ELAAs, this capability holds even for non-dispersed antennas, allowing to estimate not only the radial component of the velocity but also the transverse one. This is the concept of *velocity sensing* recently introduced in [10] when employing ELAAs working in near-field conditions, enabling to get a full picture of the target velocity and trajectory using a monostatic radar instead of multi-static radars that require challenging synchronization and expensive hardware [7]. Such a capability makes ELAAs attractive for velocity estimation, in addition to the already-known benefits of near-field operations, such as improved spatial multiplexing even in line-of-sight (LOS) conditions [4], [11], the possibility of single-anchor localization [12] and high-resolution sensing [4], [13]. To the authors' knowledge, no studies are present investigating the theoretical performance limits for velocity estimation using ELAAs in the near field. The paper [10] studies a maximum likelihood velocity estimator and its adoption for predictive beamforming applications, but it does not analyze the performance bounds and how the different system and geometrical parameters affect the estimation capability.

In this letter, we analytically derive the performance bounds for velocity estimation using ELAAs. Specifically, we show novel results according to which *(i)* the transverse velocity accuracy decreases quadratically with the target-receiver distance and *(ii)* for half-wavelength spaced arrays, it does not depend on the carrier frequency. This behavior is thus completely different from that of radial velocity estimation usually considered. Moreover, we depict the impact of the different system and geometrical parameters, highlighting the differences between near-field distance estimation and transverse velocity estimation using ELAAs.

Received 6 August 2024; revised 27 September 2024; accepted 28 September 2024. Date of publication 7 October 2024; date of current version 11 December 2024. This work was supported in part by the European Union under the Italian National Recovery and Resilience Plan (NRRP) of NextGenerationEU, partnership on "Telecommunications of the Future" (Program "RESTART") under Grant PE00000001, and in part by the EU Horizon Project TIMES under Grant 101096307. The associate editor coordinating the review of this article and approving it for publication was Y. C. Wu. *(Corresponding author: Caterina Giovannetti.)*

Caterina Giovannetti is with National Research Council (CNR-IEIIT), 40136 Bologna, Italy, also with WiLab-CNIT, 40133 Bologna, Italy, and also with DEI, University of Bologna, 40126 Bologna, Italy (e-mail: caterina.giovannetti@ieiit.cnr.it).

Nicolò Decarli is with the National Research Council (CNR-IEIIT), 40136 Bologna, Italy, and also with WiLab-CNIT, 40133 Bologna, Italy (e-mail: nicolo.decarli@ieiit.cnr.it).

Davide Dardari is with the Dipartimento di Ingegneria dell'Energia Elettrica e dell'Informazione "Guglielmo Marconi", University of Bologna, 40126 Bologna, Italy, and also with WiLab-CNIT, 40133 Bologna, Italy (e-mail: davide.dardari@unibo.it).

Digital Object Identifier 10.1109/LWC.2024.3475733

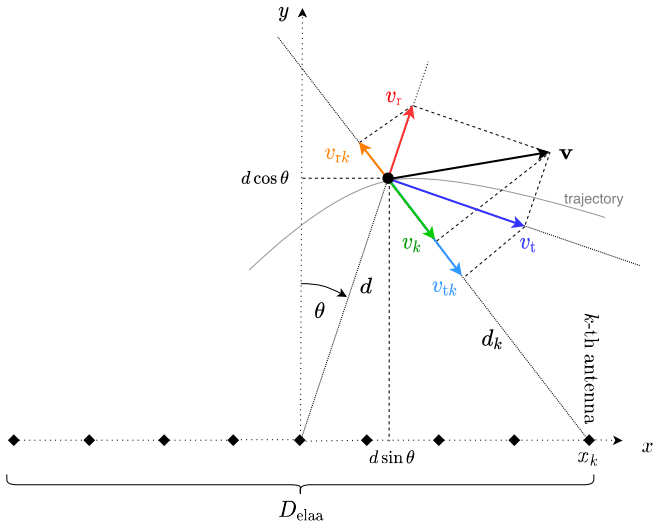

Fig. 1. Geometry of the scenario for velocity estimation with an ELAA.

II. Signal and System Model

We consider sensing of a passive point target in a 2D scenario using a single input multiple output (SIMO) monostatic radar at the base station (BS), thus with a single transmitting antenna and K receiving elements arranged according to a linear ELAA deployment. Denote with δ the antenna spacing and let us assume K to be odd. The array aperture is $D_{\text{elaa}} = (K-1)\delta$. The reference system is placed with the origin corresponding to the central element of the ELAA at the BS, which is oriented along the x-axis (see Fig. 1). Denote with $\tilde{\mathbf{p}}_k = [x_k, y_k]^\top$ the position of the k-th receiving antenna at the BS, for $k = -(K-1)/2, \ldots, (K-1)/2$, so that $x_k = k\,\delta$, $y_k = 0, \forall k$, and $x_0 = 0$ represents the array center. We assume a point target placed in position $\tilde{\mathbf{p}} = [d\sin\theta, d\cos\theta]^\top$ moving with velocity $\mathbf{v} = [v_\text{r}, v_\text{t}]^\top$ tangent to its trajectory on the plane, where v_r and v_t are the radial and transverse velocity components, respectively, with respect to the center of the ELAA (see Fig. 1). Let us now consider, for convenience, a polar coordinate system. In this case, we can write the target position as $\mathbf{p} = [d, \theta]^\top$, where $d = ||\tilde{\mathbf{p}}||$ denotes the distance between the target and the central element of the receiving ELAA at the BS, and θ denotes the angle with respect to the boresight direction of the receiving ELAA (i.e., the angle of arrival (AoA) of the signal received at the BS). Define d_k the distance between the target and the k-th receiving antenna that can be expressed as

$$d_k = \|\tilde{\mathbf{p}} - \tilde{\mathbf{p}}_k\| = d\sqrt{1 + \frac{x_k^2}{d^2} - \frac{2x_k\sin\theta}{d}}. \tag{1}$$

The central antenna element of the ELAAs, which is selected as reference for distance, angle and velocity estimation, transmits an orthogonal frequency-division multiplexing (OFDM) signal spanning N subcarriers and M OFDM symbols. At the receiver side, after classical cyclic prefix removal and FFT processing, the received signal is

$$\begin{aligned} r_{m,n,k} &= y_{m,n,k} + z_{m,n,k} \\ &= \sqrt{P}\beta_{m,n,k}\,u_{m,n}\,e^{-\text{j}2\pi f_n \tau_k}\,e^{\text{j}2\pi\nu_{n,k}mT_\text{sym}} + z_{m,n,k} \end{aligned} \tag{2}$$

where $P = P_\text{T}/N$ is the power allocated to each subcarrier, with P_T indicating the total transmit power, $u_{m,n}$ is the data symbol transmitted in the m-th OFDM symbol and n-th subcarrier, with $\mathbb{E}\{|u_{m,n}|^2\} = 1$, $T_\text{sym} = T + T_\text{cp}$ is the symbol time where T_cp stands for the cyclic prefix duration and $T = 1/\Delta f$, with Δf indicating the subcarrier spacing (SCS). The frequency $f_n \triangleq f_\text{c} + n\Delta f$ is that associated with the n-th subcarrier, $\beta_{m,n,k}$ is the channel gain coefficient, $\tau_k = \frac{d+d_k}{c}$ is the round-trip delay associated to the k-th receiving antenna, and $\nu_{n,k} = \frac{f_n}{c}(v_\text{r} + \mathbf{v}\cdot\mathbf{e}_k)$ is the round-trip Doppler shift, with $\mathbf{a}\cdot\mathbf{b}$ indicating the scalar product between vectors $\mathbf{a}$ and $\mathbf{b}$, and c the speed of light. Here, the term $\mathbf{e}_k = \mathbf{d}_k/||\mathbf{d}_k||$ is a unit norm vector denoting the direction between the k-th receiving antenna element and the target, so that $\nu_{n,k}$ includes a component which is the projection of the target's velocity along this direction for each receiving antenna. The term $z_{m,n,k}$ indicates the additive white Gaussian noise (AWGN), with $z_{m,n,k} \sim \mathcal{CN}(0, \sigma^2)$ and $\sigma^2 = k_\text{B}\,T_0 F \Delta f$, being k_B the Boltzmann constant, T_0 the reference temperature, and F the receiver noise figure. We consider the channel gain equal for all the antennas, which is reasonable for the practical size of the receiving ELAA, in particular when $d > D_\text{elaa}$ in LOS-dominated near-field scenarios [14], and small relative bandwidth $B = N\Delta f \ll f_\text{c}$, so that we can write $\beta_{m,n,k} = \beta$, $\forall m, n, k$.

Starting from the received signal (2), the BS aims at estimating the position $\mathbf{p}$ and velocity $\mathbf{v}$ through the estimation of their components $[d, \theta]$ and $[v_\text{r}, v_\text{t}]$, respectively, thanks to the use of the ELAA.

III. Velocity Estimation Performance Bounds

The optimal way of processing the receiving signal would require the joint estimation of all the unknown parameters $\boldsymbol{\Theta} = \{d, \theta, v_\text{r}, v_\text{t}\}$ from the $M \times N \times K$ observations. This would imply a very high complexity, especially when operating in the near-field region where the planar wavefront approximation does not hold. To focus here on the estimation of the radial and transverse velocity components when adopting the ELAA, we assume that the distance d and the AoA θ have already been estimated, as done also in [10]. This can be realized by exploiting the information coming from the different subcarriers (e.g., for distance estimation), and/or from the phase profile along the array caused by the spherical wavefront (e.g., for distance and angle estimation) [8]. Thus, starting from this assumption, we want to evaluate the performance limits on the estimation mean square error (MSE) of the radial and transverse velocity components v_r and v_t. Since the transmitted symbols are known by the receiver and used as pilots, in the following we consider $u_{m,n} = 1$ in (2); moreover, τ_k is known since the distance d and the angle θ have been assumed already estimated.

The velocity estimation quality in terms of MSE is lower bounded by the Cramér-Rao Lower Bound (CRLB) [15]. In this case, we have two scalar parameters to consider for the CRLB analysis, that are $\boldsymbol{\Theta} = \{v_\text{r}, v_\text{t}\}$. The (i, j)-th element of the Fisher information matrix (FIM) can be obtained as [15]

$$[\mathbf{J}]_{i,j} = \frac{2}{\sigma^2}\Re\left\{\sum_{m,n,k}\left[\frac{\partial y_{m,n,k}}{\partial \boldsymbol{\Theta}_i}\right]^*\left[\frac{\partial y_{m,n,k}}{\partial \boldsymbol{\Theta}_j}\right]\right\} \tag{3}$$

where $y_{m,n,k}$ is the noise-free version of $r_{m,n,k}$ in (2). Thus we have a 2×2 FIM in the form

$$\mathbf{J} = \begin{bmatrix} J_{v_\mathrm{r} v_\mathrm{r}} & J_{v_\mathrm{r} v_\mathrm{t}} \\ J_{v_\mathrm{t} v_\mathrm{r}} & J_{v_\mathrm{t} v_\mathrm{t}} \end{bmatrix} \tag{4}$$

with $J_{v_\mathrm{r} v_\mathrm{t}} = J_{v_\mathrm{t} v_\mathrm{r}}$, and the corresponding CRLBs on the radial and transverse velocities are given by, respectively,

$$\mathsf{CRLB}^{(v_\mathrm{r})} = \frac{1}{\det \mathbf{J}} J_{v_\mathrm{t} v_\mathrm{t}} \qquad \mathsf{CRLB}^{(v_\mathrm{t})} = \frac{1}{\det \mathbf{J}} J_{v_\mathrm{r} v_\mathrm{r}} \tag{5}$$

where $\det \mathbf{J} = J_{v_\mathrm{r} v_\mathrm{r}} J_{v_\mathrm{t} v_\mathrm{t}} - J^2_{v_\mathrm{t} v_\mathrm{r}}$.

According to the geometry of Fig. 1, we can project the radial and transverse velocity components along the direction $\mathbf{e}_k$ by obtaining the projections $v_{\mathrm{r}k}$ and $v_{\mathrm{t}k}$, respectively. It holds

$$v_k = v_{\mathrm{r}k} + v_{\mathrm{t}k} \tag{6}$$

where v_k is the projection of the velocity $\mathbf{v}$ along the direction $\mathbf{e}_k$. Then, we can write

$$\nu_{n,k} = \frac{f_n}{c}(v_\mathrm{r} + v_k). \tag{7}$$

The projections $v_{\mathrm{r}k}$ and $v_{\mathrm{t}k}$ can be obtained as [10]

$$v_{\mathrm{r}k} = q_k v_\mathrm{r} \tag{8}$$

$$v_{\mathrm{t}k} = p_k v_\mathrm{t} \tag{9}$$

where

$$q_k = \frac{d - x_k \sin\theta}{d_k} = \frac{1 - \frac{x_k \sin\theta}{d}}{\sqrt{1 + \frac{x_k^2}{d^2} - \frac{2x_k \sin\theta}{d}}} \tag{10}$$

$$p_k = \frac{x_k \cos\theta}{d_k} = \frac{x_k \cos\theta}{d\sqrt{1 + \frac{x_k^2}{d^2} - \frac{2x_k \sin\theta}{d}}}. \tag{11}$$

By substituting (8) and (9) in (6), and considering (7) in the model (2), we can compute the derivatives in (3) and obtain the components of the FIM

$$J_{v_\mathrm{r} v_\mathrm{r}} = \sum_n I_n \sum_k (1 + q_k)^2 \tag{12}$$

$$J_{v_\mathrm{t} v_\mathrm{t}} = \sum_n I_n \sum_k p_k^2 \tag{13}$$

$$J_{v_\mathrm{t} v_\mathrm{r}} = \sum_n I_n \sum_k p_k (1 + q_k) \tag{14}$$

where

$$I_n = \frac{2\pi^2 f_n^2 \, M \, \mathsf{SNR} \left(M^2 - 1\right) T_{\mathrm{sym}}^2}{3c^2} \tag{15}$$

and we defined the signal-to-noise ratio (SNR) as $\mathsf{SNR} = P\beta^2/\sigma^2$. Considering the practical case $d > D_{\mathrm{elaa}}$, it holds $J_{v_\mathrm{r} v_\mathrm{r}} J_{v_\mathrm{t} v_\mathrm{t}} \gg J^2_{v_\mathrm{t} v_\mathrm{r}}$ so that $\det \mathbf{J} \approx J_{v_\mathrm{r} v_\mathrm{r}} J_{v_\mathrm{t} v_\mathrm{t}}$ and we have $\mathsf{CRLB}^{(v_\mathrm{r})} \approx 1/J_{v_\mathrm{r} v_\mathrm{r}}$ and $\mathsf{CRLB}^{(v_\mathrm{t})} \approx 1/J_{v_\mathrm{t} v_\mathrm{t}}$.[1] The limit for $d \to \infty$ in (10) is $q_k \to 1$ so that the right-hand summation in (12) tends to $4K$. Thus, for the estimation of the radial velocity component v_r, the information (12) tends to the inverse of the traditional CRLB for velocity estimation in far-field conditions, which is given by [16]

$$\mathsf{CRLB}^{(v_\mathrm{r})} = \frac{3c^2}{8\pi^2 f_\mathrm{c}^2 \, MNK \mathsf{SNR} \left(M^2 - 1\right) T_{\mathrm{sym}}^2} \tag{16}$$

where we considered $f_n \approx f_\mathrm{c}$ since $B \ll f_\mathrm{c}$. Notice that $(M^2 - 1) T_{\mathrm{sym}}^2$ is approximately the squared signal duration T_{obs}^2, and in (16) it is highlighted the SNR gain MNK obtained thanks to the exploitation of M symbols, N subcarriers and K antennas for the estimation. When $\theta = 0$, (12) becomes

$$J_{v_\mathrm{r} v_\mathrm{r}} = \frac{2\pi^2 f_\mathrm{c}^2 MN \mathsf{SNR} \left(M^2 - 1\right) T_{\mathrm{sym}}^2}{3c^2} \sum_k \left(1 + \frac{1}{\sqrt{1 + k^2 \frac{\delta^2}{d^2}}}\right)^2. \tag{17}$$

Interestingly, the information on the target's radial velocity reduces as the distance d decreases, since $k^2\delta^2/d^2 > 0$, resulting in an SNR gain lower than K for a small distance. This is reasonable since when the target approaches the array, the antennas farther from the array center sense the target in a direction different from that corresponding to the radial velocity, which is defined according to the reference central element. However, for practical array dimensions and operating distances (in particular, when the distance becomes higher than the largest x_k, i.e., than the array aperture D_{elaa}), the term $k^2\delta^2/d^2$ is small. Therefore, as far as the distance d exceeds D_{elaa}, we have $1/J_{v_\mathrm{r} v_\mathrm{r}} \to \mathsf{CRLB}^{(v_\mathrm{r})}$ in (16) which does not depend on the distance d and on the array aperture. Thus, no differences are experienced between far-field and near-field radial velocity estimation quality.

For what concerns the transverse velocity, its estimation at a large distance is not possible; specifically, we have $p_k \to 0$ for $d \to \infty$ (in practice, when $d \gg D_{\mathrm{elaa}}$) so that $J_{v_\mathrm{t} v_\mathrm{t}} \to 0$ and no information can be retrieved. In fact, when the target is far, the whole array sees it under a single direction, which is that of the radial velocity. Differently, when the array aperture increases and/or the distance decreases, we have $p_k \neq 0$, and transverse velocity estimation becomes feasible. Therefore, the possibility of gathering information on the transverse velocity can be attributed to the possibility of projecting the target velocity along the set of directions corresponding to the different antennas of the array. The information on transverse velocity is maximum on the boresight direction of the ELAA according to (13) and (11) (i.e., $\theta = 0$); differently from the radial velocity, it is not possible to estimate the transverse velocity when $\theta = \pm\frac{\pi}{2}$. In fact, in this case, the direction $\mathbf{e}_k$ is the same for all the antennas and corresponds to the radial direction, so no further information becomes available rather than the radial velocity. The same behavior is experienced in near-field distance estimation with uniform linear arrays (ULAs), which is not possible for $\theta = \pm\frac{\pi}{2}$ [17]. For the case of transverse velocity estimation, we can write for $\theta = 0$

$$J_{v_\mathrm{t} v_\mathrm{t}} = \frac{2\pi^2 f_\mathrm{c}^2 \, MN \mathsf{SNR} \left(M^2 - 1\right) T_{\mathrm{sym}}^2 \delta^2}{3c^2 \, d^2} \sum_k \frac{k^2}{1 + k^2 \frac{\delta^2}{d^2}} \tag{18}$$

which decreases with the square of the distance d for fixed SNR. Considering the practical case $d > D_{\mathrm{elaa}}$, which also allows to define the SNR according to (15), the term $k^2\delta^2/d^2$ is generally small, and the following approximate expression

[1] Exploiting the 2nd order Taylor expansion for q_k, we have that $q_k \to 1$ since the term x_k^2/d^2 is small for $d > D_{\mathrm{elaa}}$ and $\cos^2\theta$ spans between 0 and 1. Using the same expansion for p_k, the ratio between $J^2_{v_\mathrm{t} v_\mathrm{r}}$ and $J_{v_\mathrm{r} v_\mathrm{r}} J_{v_\mathrm{t} v_\mathrm{t}}$ results less than 0.08 when $d > D_{\mathrm{elaa}}$. This leads to the conclusion that the estimation of the radial and the transverse velocity components are practically decoupled in this configuration.

is obtained

$$J_{v_\mathrm{t}v_\mathrm{t}} \approx \frac{\pi^2 f_\mathrm{c}^2\, MNK\mathsf{SNR}\left(M^2-1\right)T_\mathrm{sym}^2\left(K^2-1\right)\delta^2}{18c^2\, d^2} \approx \frac{\pi^2 f_\mathrm{c}^2\, MNK\mathsf{SNR}\, T_\mathrm{obs}^2 D_\mathrm{elaa}^2}{18c^2 d^2}. \quad (19)$$

As for the traditional CRLB on radar-based velocity estimation in (16), the information on the transverse velocity is proportional to the squared signal duration. Larger carrier frequency f_c is beneficial for both radial and transverse velocity estimation. The adoption of a proper array aperture D_elaa can be traded to achieve the required transverse velocity accuracy depending on the operating distance d, while the SNR and the symbol time have the same impact on both the components.

Expression (19) shows a deep difference between what happens in the near field for distance estimation and transverse velocity estimation. In fact, in near-field distance estimation, the CRLB is proportional to $d^2/f_\mathrm{c}^2 D_\mathrm{elaa}^4$ [17]; as a result, in that case, the root-CRLB is inversely proportional to the Fraunhofer distance $d_\mathrm{ff} = 2D_\mathrm{elaa}^2/\lambda$, with $\lambda = c/f_\mathrm{c}$. Therefore, increasing the array aperture D_elaa (i.e., number of antennas, antenna spacing) and/or the carrier frequency is beneficial for the estimation quality, with a larger impact of the array aperture. Instead, in transverse velocity estimation using ELAAs, the parameters affecting the quality are the same according to (19), but they influence the bound all with the second power. Differences are evident when considering a half-wavelength spaced array ($\delta = \lambda/2$). In this case, the information on the transverse velocity is

$$J_{v_\mathrm{t}v_\mathrm{t}} \approx \frac{\pi^2\, MNK\mathsf{SNR}\left(M^2-1\right)T_\mathrm{sym}^2\left(K^2-1\right)}{72d^2} \quad (20)$$

which does not depend on the carrier frequency, differently from the radial velocity estimation or what happens for near-field distance estimation.

IV. Numerical Results

We present some results concerning the quality of velocity estimation using a linear ELAA. If not differently specified, we consider $f_\mathrm{c} = 28\,\mathrm{GHz}$, $K = 101$ antennas, $N = 1$ and a fixed SNR of $0\,\mathrm{dB}$. A packet with $M = 14$ OFDM symbols is considered, and symbol time $T_\mathrm{sym} = 16.6\,\mathrm{ms}$. According to the expressions reported in Section III, the presented root-CRLB curves will scale with $\sqrt{N}$ when considering $N > 1$.

Fig. 2 shows the root-CRLB for the radial velocity estimation in (5)-left as a function of the distance d, for a small distance from the array. Markers indicate the approximation obtained as $\sqrt{1/J_{v_\mathrm{r}v_\mathrm{r}}}$, with $J_{v_\mathrm{r}v_\mathrm{r}}$ given by (17), showing that it is very tight for the condition of interest. The traditional far-field CRLB according to (16) is reported for comparison. Results are given for different apertures D_elaa, but with the same number of antennas K; this choice allows to consider a fixed overall received power, thus characterizing the impact of the array aperture under a constant number of observations MNK and thus SNR gain. As it is possible to notice, a small deviation from the far-field CRLB is experienced only at very small distance from the array, in particular, for a distance below the array aperture D_elaa, region also known as *geometric near field* [11].

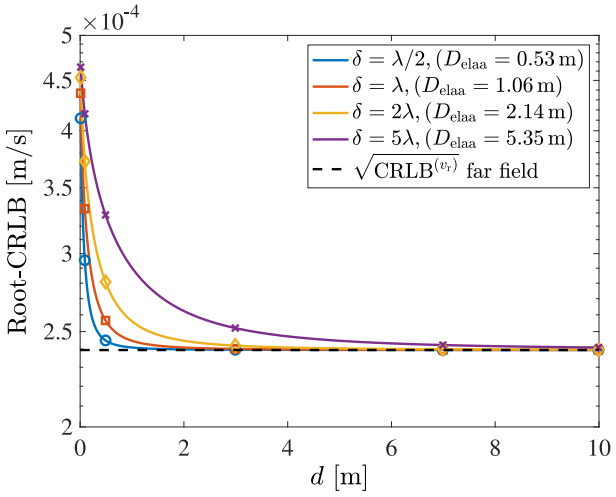

Fig. 2. Root-CRLB for the radial velocity as a function of the distance d for different apertures D_elaa. Markers stand for $\sqrt{1/J_{v_\mathrm{r}v_\mathrm{r}}}$ in the same setting.

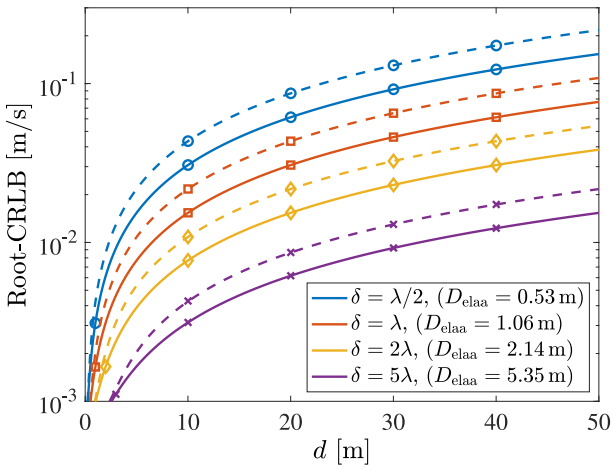

Fig. 3. Root-CRLB for the transverse velocity as a function of the distance d for different apertures D_elaa. Continuous lines (–) are for $\theta = 0$; dashed lines (- -) are for $\theta = 45°$. Markers stand for $\sqrt{1/J_{v_\mathrm{t}v_\mathrm{t}}}$ in the same setting.

In Fig. 3 the root-CRLB for the transverse velocity in (5)-right is reported as a function of the distance d, considering $\theta = 0$ and $\theta = 45°$. Again, the comparison between the exact root-CRLB and its approximation $\sqrt{1/J_{v_\mathrm{t}v_\mathrm{t}}}$ (markers) shows a very good agreement. It can be noticed that the accuracy decreases as the distance d increases, as well as when the angle increases. The array aperture D_elaa has a fundamental role in achieving a good estimation quality.

Fig. 4 compares the radial and transverse velocity accuracy in terms of root-CRLB as a function of the distance d for a fixed number of antennas K, $\delta = \lambda/2$, $\theta = 0$, and two different carrier frequencies, i.e., $f_\mathrm{c} = 6\,\mathrm{GHz}$ and $f_\mathrm{c} = 28\,\mathrm{GHz}$. Thus, the two conditions translate in two different array apertures D_elaa. It is possible to notice that the radial accuracy is close to the traditional far-field CRLB, and it is always higher than the transverse one. In fact, by comparing (16) and (19) it can be seen that when $d = D_\mathrm{elaa}/(4\sqrt{3})$, the estimation quality for the radial velocity equals the estimation quality for the transverse one, at $\theta = 0$. Thus, an operating distance smaller than the array aperture D_elaa is required to achieve a balance in

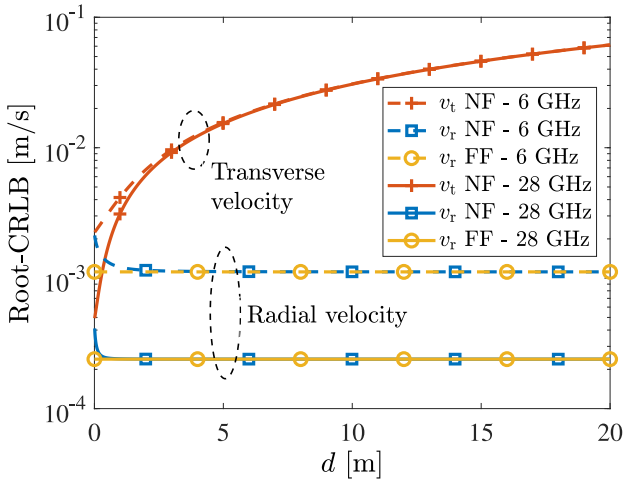

Fig. 4. Root-CRLB for the radial and transverse velocities in near-field (NF) conditions. Comparison with the far-field (FF) CRLB in (16).

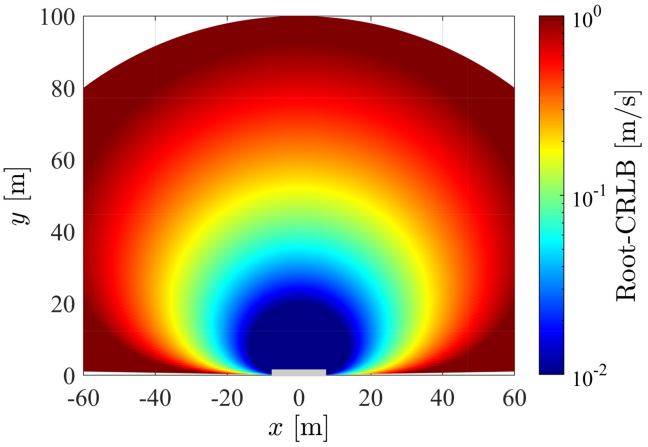

Fig. 5. Distribution of the root-CRLB for transverse velocity on the 2D plane. Array of aperture $D_{\text{elaa}} \approx 0.5\,\text{m}$ centered in $[0, 0]$ deployed along the x axis.

terms of estimation quality among the different components of the velocity. The transverse velocity accuracy does not depend on the carrier frequency, since we are comparing the results considering half-wavelength antenna spacing; differently, the estimation quality for the radial velocity improves as the carrier frequency increases.

Finally, a 2D map considering the distribution of the root-CRLB for the transverse velocity in the semi-plane in front of the ELAA is reported in Fig. 5. We considered a transmit power $P_{\text{T}} = 23\,\text{dBm}$ and a receiver noise figure $F = 9\,\text{dB}$. This allows to include the impact of the path loss in the SNR. A target with radar cross section of $1\,\text{m}^2$ is assumed, and $0\,\text{dBi}$ gain antennas. As evident, the transverse accuracy decreases as the distance from the array increases due to the combined effect of the term d^2 in (19) and of the SNR scaling; moreover, it deteriorates at large angles, due to the use of the linear array.

V. Conclusion

This letter laid the foundation for estimating radial and transverse velocity components of a moving target using a linear ELAA, by analytically deriving the corresponding CRLBs. The results show that the accuracy of transverse velocity estimation decreases with the square of the target-antenna distance, and it is unaffected by the carrier frequency when using a half-wavelength spaced array. This behavior contrasts with the radial velocity component and differs from near-field distance estimation. In fact, the possibility of gathering information on the transverse velocity can be mostly attributed to the proximity of the target and to the geometrical arrangement of the array relative to the target's position. Hence, the array aperture plays a crucial role in achieving a satisfactory performance.

References

[1] F. Liu et al., "Integrated sensing and communications: Toward dual-functional wireless networks for 6G and beyond," *IEEE J. Sel. Areas Commun.*, vol. 40, no. 6, pp. 1728–1767, Jun. 2022.
[2] S. J. Orfanidis, *Electromagnetic Waves and Antennas*. New Brunswick, NJ, USA: Rutgers Univ., 2008.
[3] D. Dardari and N. Decarli, "Holographic communication using intelligent surfaces," *IEEE Commun. Mag.*, vol. 59, no. 6, pp. 35–41, Jun. 2021.
[4] M. Cui, Z. Wu, Y. Lu, X. Wei, and L. Dai, "Near-field MIMO communications for 6G: Fundamentals, challenges, potentials, and future directions," *IEEE Commun. Mag.*, vol. 61, no. 1, pp. 40–46, Jan. 2023.
[5] Z. Wang et al., "A tutorial on extremely large-scale MIMO for 6G: Fundamentals, signal processing, and applications," *IEEE Commun. Surveys Tuts.*, vol. 26, no. 3, pp. 1560–1605, 3rd Quart., 2024.
[6] A. Sakhnini et al., "Near-field coherent radar sensing using a massive MIMO communication testbed," *IEEE Trans. Wireless Commun.*, vol. 21, no. 8, pp. 6256–6270, Aug. 2022.
[7] S. K. Dehkordi et al., "Multistatic parameter estimation in the near/far field for integrated sensing and communication," *IEEE Trans. Wireless Commun.*, early access, Sep. 18, 2024, doi: 10.1109/TWC.2024.3458048.
[8] Z. Wang, X. Mu, and Y. Liu, "Near-field integrated sensing and communications," *IEEE Commun. Lett.*, vol. 27, no. 8, pp. 2048–2052, Aug. 2023.
[9] Q. He et al., "Cramer-Rao bound for target velocity estimation in MIMO radar with widely separated antennas," in *Proc. 42nd Annu. Conf. Inf. Sci. Syst.*, 2008, pp. 123–127.
[10] Z. Wang, X. Mu, and Y. Liu, "Near-field velocity sensing and predictive beamforming," *IEEE Trans. Veh. Technol.*, early access, Sep. 4, 2024, doi: 10.1109/TVT.2024.3454481.
[11] N. Decarli and D. Dardari, "Communication modes with large intelligent surfaces in the near field," *IEEE Access*, vol. 9, pp. 165648–165666, 2021.
[12] A. Guerra et al., "Near-field tracking with large antenna arrays: Fundamental limits and practical algorithms," *IEEE Trans. Signal Process.*, vol. 69, pp. 5723–5738, Aug. 2021.
[13] H. Chen et al., "6G localization and sensing in the near field: Features, opportunities, and challenges," *IEEE Wireless Commun.*, vol. 31, no. 4, pp. 260–267, Aug. 2024.
[14] E. Björnson, O. T. Demir, and L. Sanguinetti, "A primer on near-field beamforming for arrays and reconfigurable intelligent surfaces," in *Proc. Asilomar Conf. Signals, Syst., Comput.*, 2021, pp. 105–112.
[15] S. M. Kay, *Fundamentals of Statistical Signal Processing: Estimation Theory*. Upper Saddle River, NJ, USA: Prentice-Hall, 1993.
[16] M. Braun, *OFDM Radar Algorithms in Mobile Communication Networks*, Karlsruher Inst. für Technologie, Karlsruhe, Germany, 2014.
[17] M. N. E. Korso, R. Boyer, A. Renaux, and S. Marcos, "Conditional and unconditional Cramér–Rao bounds for near-field source localization," *IEEE Trans. Signal Process.*, vol. 58, no. 5, pp. 2901–2907, May 2010.

Open Access funding provided by 'Consiglio Nazionale delle Ricerche-CARI-CARE-ITALY' within the CRUI CARE Agreement